Production, cellular structure and thermal conductivity of microcellular (methyl methacrylate)–(butyl acrylate)–(methyl methacrylate) triblock copolymers

Jose Antonio Reglero Ruiz, Cristina Saiz-Arroyo, Michel Dumon, Miguel A Rodríguez-Perez and Leo Gonzalez

Abstract

Microcellular foaming of a (methyl methacrylate)–(butyl acrylate)–(methyl methacrylate) triblock copolymer was carried out by means of supercritical CO_2 in a single-step process. The experiments were performed at 40 °C using a pressure of 300 bar (30 MPa) during 24 h. The depressurization times were modified from 2 to 30 min, leading to cell sizes from 10 to 100 μm, and relative densities from 0.11 to 0.17. It was found that the key parameter to control cell size and density was depressurization time: longer depressurization times generated larger cell sizes and lower densities. The thermal conductivity of these materials was measured using the transient plane source technique, and it was found that this decreased as the density was reduced. Various models for the prediction of thermal conductivity by conduction were tested. It was found that all the models underestimated the experimental results due to a significant contribution of radiation heat flow for these materials.

Keywords: microcellular foams; thermal conductivity; triblock copolymers; cellular structure

INTRODUCTION

Microcellular foams are defined as having average cell sizes in the range 1–10 μm, and cell densities of the order of 10^9–10^{15} cells cm^{-3}. Such structures were proposed by Suh and co-workers,[1,2] and it is now well known that inert gases such as CO_2 can be used to foam amorphous polymeric materials. The low critical parameters of supercritical CO_2 (31.1 °C and 73.8 bar (7.38 MPa)) offer many advantages, such as tuneable solvent power, plasticization of glassy polymers and higher diffusion rates.[3,4]

To produce a microcellular structure, there are two main well-established processes. In the first process, a single-step process, a polymer is saturated with CO_2 in the supercritical regime, for a fixed time period and temperature. After saturation, the sample is depressurized to atmospheric pressure at a constant temperature, taking advantage of the swelling and plasticization of the polymer, which reduce the glass transition temperature (T_g), allowing gas expansion. In this method, the microstructure is controlled by changing the processing temperature and depressurization rates. In the second process, a two-step process, a polymer is saturated with supercritical CO_2 at high pressure and low temperature. Next, the polymer/gas mixture is quenched into a supersaturated state by reducing drastically the pressure. Finally, after removing the sample from the vessel, the polymer is foamed by heating to a temperature above T_g, leading to nucleation and cell growth. Foaming temperature and foaming time are the key parameters to adjust the cellular structure of the final product.[5] Both processes have been employed to obtain several microcellular polymers, including polystyrene,[6] polycarbonate,[7] polystyrene-*co*-(methyl methacrylate)[8] and poly(methyl methacrylate) (PMMA).[9,10] Block copolymers have also been used as starting materials in the supercritical foaming process in several recent investigations.[11,12]

In a similar way, the study of various properties, especially mechanical properties, has attracted considerable attention. Tension and compression tests have been carried out on microcellular polymers, such as polystyrene, PMMA and other amorphous polymers such as polyethersulfone and polyphenylsulfone, correlating structural parameters (foam density, cell size, etc.) with mechanical data.[13–15]

Thermal properties, especially thermal conductivity, have been much investigated for cellular materials,[16,17] but there is a lack of knowledge when the microcellular range is considered. The work reported here focused on the thermal conductivity of a collection of microcellular foams of a poly(methyl methacrylate)–poly(butyl acrylate)–poly(methyl methacrylate) triblock copolymer, which

* *Correspondence to: Jose Antonio Reglero Ruiz, Laboratoire de Chimie de Polymères Organiques (LCPO), IPB, 16 Avenue Pey-Berland, Université Bordeaux 1, 33607 Pessac Cedex, France. E-mail: reglero-ruiz@enscpb.fr*

a *Laboratoire de Chimie de Polymères Organiques (LCPO), IPB, 16 Avenue Pey-Berland, Université Bordeaux 1, 33607 Pessac Cedex, France*

b *Cellular Materials Laboratory (CellMat), Condensed Matter Physics Department, University of Valladolid, 47011 Valladolid, Spain*

c *School of Naval Engineering (ETSI), Av Arco de la Victoria s/n, University of Madrid, 28040 Madrid, Spain*

is employed as an additive in several applications and presents a very high affinity to CO_2.[18] The foaming behaviour of PMMA homopolymer has been analysed in depth, and in our case, the originality of the work is based on the features of this special triblock copolymer, which shows a nanostructured assembly in which the methacrylate and butyl acrylate blocks can be self-organized in various ways. Several AFM and transmission electron microscopy images showing this effect can be found elsewhere.[19,20] This nanostructured triblock copolymer is normally used to enhance mechanical properties as an additive in materials such as epoxy resins, but no influence of the nano-assembly on the foaming behaviour has been reported. In the study reported here, we analysed the effect of this self-assembly, which is not observed in PMMA homopolymer, on the main foaming characteristics, especially average cell size and foam density. Moreover, for the determination of the thermal conductivity, a new experimental technique, the transient plane source (TPS) technique, was employed. The TPS technique is one of the most important transitory methods to measure thermal conductivity, and it is based on the analysis of the transient term solution of the heat conduction equation, which relates change in temperature with time. These methods have several advantages in comparison with the steady-state methods, such as a wide measuring range (*ca* 0.02 to 400 W m^{-1} K^{-1}), the possibility of measuring properties of inhomogeneous and/or anisotropic materials and the additional possibility of measuring small samples. Furthermore, measurements are in general fast and they can be performed in localized parts of samples. Finally, it is also interesting to comment that, in the last few years, various types of materials (butadiene rubber compounds, pineapple leaf fibre-reinforced composites, highly porous building materials and in particular polymer foams and metal foams) have been characterized using the TPS technique.[21–25]

EXPERIMENTAL

Materials

The (methyl methacrylate)–(butyl acrylate)–(methyl methacrylate) (MAM) triblock copolymer was kindly supplied by Altuglas Company (La Garenne-Colombes, France) in the form of pellets. This resin is specially designed as an additive for improving the mechanical properties, especially impact resistance, of several epoxy systems. The chemical structure of the triblock copolymer is shown in Fig. 1. The main characteristics of the material are as follows: bulk density ρ_s of 1.18 g cm^{-3}, T_g of *ca* 374 K and weight-average molecular weight M_w of 99 000 g mol^{-1}. The relative amounts of methyl methacrylate, butyl acrylate and methyl methacrylate blocks were 30 : 40:30 (wt%). Carbon dioxide (99.9%) was obtained from Air Liquide (Cergy Pontoise, France).

Solids preparation

As-received pellets were injected-moulded into sheets (50 × 15 mm^2) of 3 mm thickness using a small-scale injection moulding machine developed by DSM Xplore. The working temperature was fixed at 250 °C, whereas the mould temperature was 60 °C. Although the working temperature was relatively high, material was not degraded due to the short processing time. Moreover, high processing temperatures allowed a better injection process. The injection pressure was fixed at 12 bar (1.2 MPa). Samples obtained showed a good surface appearance as well as a good injection behaviour, with no presence of air bubbles inside the sheets.

Figure 1. Chemical structure of the MAM triblock copolymer.

Microcellular foaming

Microcellular foaming experiments were carried out using a high-pressure reactor provided by TOP Industry, with a capacity of 300 cm^3 and capable of operating at a maximum temperature of 250 °C and 400 bar (40 MPa). The reactor was equipped with a pressure pump controller provided by Teledyne ISCO, which was controlled automatically to keep the temperature and pressure at the desired values.

Foaming experiments were performed in a single-step batch process. First, samples were saturated with supercritical CO_2 at 40 °C at a constant pressure of 300 bar (30 MPa) during 24 h. Saturation time was selected in order to ensure the complete dissolution of CO_2 in the polymer.[26,27] It is well known that depression of T_g is induced by supercritical CO_2 for several amorphous polymers,[28] showing a linear T_g–P relation, and for this reason a foaming temperature of 40 °C was chosen to perform the experiments. In our case, similar temperatures, times and pressures to those previously used for PMMA were selected.[29] A saturation pressure of 300 bar (30 MPa) and a period of 24 h were selected, in order to ensure complete dissolution of the gas in the polymer. For the saturation temperature, a value of 40 °C was chosen. For this saturation temperature, the plasticization effect in the butyl acrylate block can be neglected, due the low T_g of the butyl acrylate central block (close to −50 °C). Using this saturation temperature has two main objectives: first, foaming at temperatures close to T_g of the methacrylate groups ensures the growth of cells during the gas expansion; second, gas solubility increases at lower temperatures, which means that the quantity of gas absorbed for the sample is higher, and more nucleation sites are formed. After the equilibrium amount of gas had been absorbed by the samples, microcellular foaming was produced releasing the pressure at different rates, from 2 to 30 min, keeping the temperature inside the reactor fixed. After foaming, samples were removed from the reactor, and the originally transparent sheets had become opaque and white.

Characterization

Foam density

Foam density ρ_f was determined using the water-displacement method, based on the Archimedes principle. It is important to note that the outer skin was removed mechanically, using a rotary polishing machine equipped with abrasive discs based on alumina and diamond. This procedure was carried out in order to obtain more precisely the density of the cellular structure, and due to the closed cell structure of the foam samples, there was no uptake of water by the samples during measurements. The relative foam density, i.e. the ratio of the foam density (ρ_f) to that of the solid polymer (ρ_s), was also calculated. At least three measurements were carried out for each sample produced.

SEM observations

Cellular structure was analysed by means of SEM (Hitachi S-3000N). For the preparation of the samples, foams were frozen in liquid

nitrogen and fractured to ensure that the microstructure remained intact. For the observations, surfaces were coated with gold using a sputter coater (EMSCOPE SC 500) in argon atmosphere. The micrographs obtained were analysed to measure cell sizes and the presence of the solid outer skin produced. To perform the calculations, a total of six SEM images from different zones of the sample were picked, mapping the whole area of observation. Cell size ϕ was obtained from direct observation of each SEM image, using a minimum of 100 cells in each calculation. Cell density N_C (cells cm^{-3}) was calculated using the following equation:[28]

$$N_C \cong \frac{6[(\rho_s/\rho_f) - 1]}{\pi\phi^3} \quad (1)$$

Thermal conductivity: TPS technique

In the TPS method, a round and plane heat source is used. It behaves as a transient plane source working simultaneously as a temperature sensor. This element consists of an electrical conducting pattern of thin nickel foil (10 μm thick) in the form of double spiral, inserted between two insulating layers made of Kapton (70 μm thick), so the final sensor thickness is 150 μm. The TPS element is located between two samples with both sensor faces in contact with the two sample surfaces. Two samples of similar characteristics are required for this purpose. To perform the experiments a constant electric power is supplied to the hot-disc sensor. The increase in temperature $\Delta T(t)$ is directly related to the variation in the sensor resistance $R(t)$ by the equation

$$R(t) = R_0[1 + \alpha\Delta T(t)] \quad (2)$$

where R_0 is the disc resistance at the beginning of the recording (initial resistance) and α is the temperature coefficient of resistance of the nickel foil.

Assuming an infinite sample and the conductive pattern being in the *XY* plane of a coordinate system, the temperature rise at a point (*XY*) at time *t* is obtained by solving the equation for the heat conduction, which relates change in temperature with time.[30,31] In the particular case of our sensor geometry, *n* concentric ring sources, the spatial average $\overline{\Delta T(\tau)}$ can be obtained through the equation

$$\overline{\Delta T(\tau)} = P_0(\pi^{3/2}a\lambda)^{-1}D(\tau) \quad (3)$$

where P_0 is a Bessel function, $D(\tau)$ is a geometric function characteristic of the number n of concentric rings and $\overline{\Delta T(\tau)}$ is the temperature increase of the sensor expressed in terms of only one variable τ, defined as

$$\tau = \left(\frac{t}{\theta}\right)^{1/2}; \ \theta = \frac{a^2}{k} \quad (4)$$

where t is the measurement time from the start of transient heating, θ is the characteristic time, which depends on parameters of both the sensor and the sample, a is the sensor radius and k is the thermal diffusivity of the sample. Thermal resistance can be obtained by fitting the experimental data to the straight line given by Eqn (2), and thermal diffusivity is calculated from Eqn (4) taking into account the θ value determined experimentally.

To perform the experiments, the TPS sensor was embedded between two samples of the same material. A sensor of radius 2.001 mm was chosen. The thickness of the microcellular samples varied between 6 and 8 mm, depending of the final density, ensuring that the boundary conditions to perform the transient plane source experiments were verified (see Eqns (4) and (5)). The skin of the samples was removed, as in the density experiments.

Output power (*W*) was selected between 0.004 and 0.005 W and total measurement time (*t*) varied between 12 and 18 s for all samples analysed. At least three measurements were carried out for each sample.

RESULTS AND DISCUSSION

Density

The density results are shown in Fig. 2, as a function of depressurization time. It can be seen that density decreases with depressurization time, from 0.20 g cm^{-3} corresponding to 2 min of depressurization time, to a minimum value of 0.13 g cm^{-3} for 30 min of depressurization time. Moreover, density values for 10 and 30 min of depressurization time are similar (0.15 and 0.13 g cm^{-3}, respectively), showing that this parameter is not greatly influenced by depressurization time above 10 min. It is important to notice the low density values for all the samples fabricated (density of bulk material was 1.18 g cm^{-3}), which leads to values of gas volume fraction from 82 to 88%. This indicates the high quantity of gas absorbed by the samples during the process, mainly due to the great affinity expected between the methacrylate groups and the supercritical CO_2.

Cellular structure

Several SEM micrographs showing the cellular structure of the foams produced are shown in Fig. 3. As can be seen, the cell size is smaller at shorter depressurization time (10 μm; Fig. 3(a)), whereas increasing the depressurization time leads to greater cell size (100 μm; Fig. 3(b)). It is clear that increasing the depressurization time allows nucleated cells more time to develop. However, from Fig. 3(b) it is clear that large cells do not retain a spherical geometry, and homogeneity is much lower than that observed in foams with small cell sizes. It is important to remark that density decreases as cell size increases, due to coalescence, which occurs at larger depressurization rates. As expected, all the structures obtained are closed-cell and, and as seen before, present a good homogeneity.

Figure 4 shows the dependence of cell size on depressurization rate, measured directly from SEM micrographs. Error bars are included to reflect the homogeneity observed in the samples. Table 1 presents the data derived from SEM observations, together with the expansion ratio and cell density calculated from Eqn (1). It is evident that cell density decreases with depressurization time,

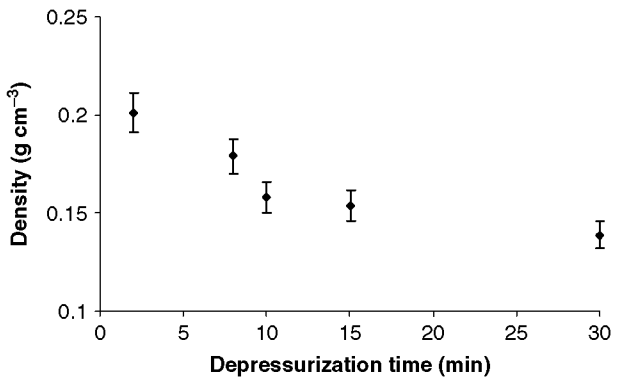

Figure 2. Foam density as a function of depressurization time. (Foaming conditions: 300 bar (30 MPa) and 40 °C).

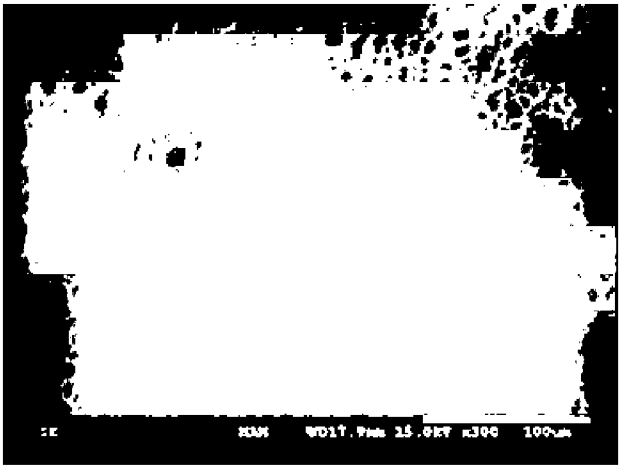

(a)

(b)

Figure 3. SEM micrographs of samples produced at various depressurization times: (a) 2 min; (b) 30 min.

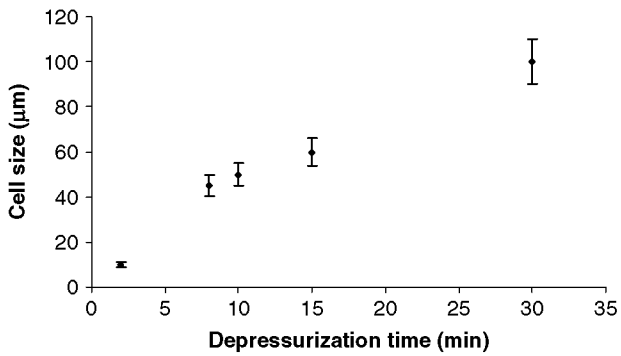

Figure 4. Dependence of cell size on depressurization time.

with values of 9.31×10^9 cells cm^{-3} at 2 min of depressurization time and 1.44×10^7 cells cm^{-3} at 30 min of depressurization time. There is a clear correlation between values of cell size, foam density and cell density, showing the effect of depressurization time on cellular structure. As depressurization time increases, cells are allowed to grow, leading to larger cell sizes, lower densities as well as lower cell densities, and phenomena such as coalescence occur, resulting in samples with low homogeneity, as seen in Fig. 3(b).

Table 1. Values of foam density, relative density, average cell size and cell density for all samples fabricated (experimental error is 5% in all cases)

Depressurization time (min)	ρ_f (g cm^{-3})	Relative density	ϕ (μm)	N_c (cells cm^{-3})
2	0.201	0.170	9	9.31×10^9
8	0.179	0.152	44	1.17×10^8
10	0.158	0.134	51	9.89×10^7
15	0.153	0.130	61	5.94×10^7
30	0.138	0.117	98	1.44×10^7

Table 2. Thermal conductivity of the microcellular foam samples (experimental error is 3%)

Depressurization time (min)	Measurement time (s)	Output power (W)	Thermal conductivity (W m^{-1} K^{-1})
2	15	0.0045	0.0628
8	15	0.004	0.0627
10	15	0.004	0.0589
15	15	0.0045	0.0599
30	18	0.0045	0.0556

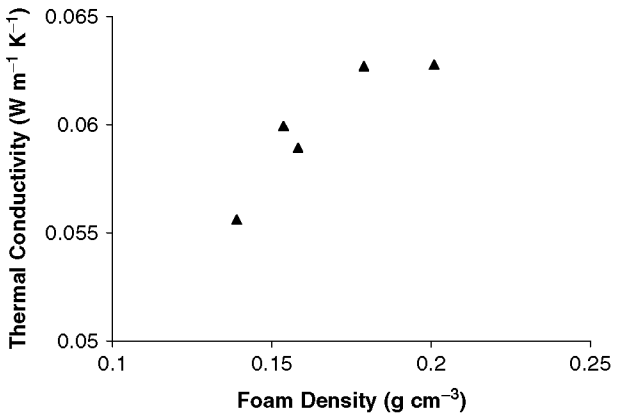

Figure 5. Thermal conductivity as a function of foam density.

Thermal conductivity

Experimental results

Table 2 summarizes the experimental results obtained for thermal conductivity. It can be seen that the thermal conductivity of the microcellular foam samples is reduced compared to the solid material ($\lambda_{MAM} \approx 0.213$ W m^{-1} K^{-1}, measured using the same technique, with 0.008 W of output power and 18 s of measurement time). This reduction is due to the effect of the gas inside the cells, and it is usual for cellular materials. It is important to notice that all the experiments performed present very good repeatability, with no great variations in the measured thermal conductivity values. Figure 5 shows the thermal conductivity values as a function of foam density. As can be seen, the thermal conductivity increases as a function of density.

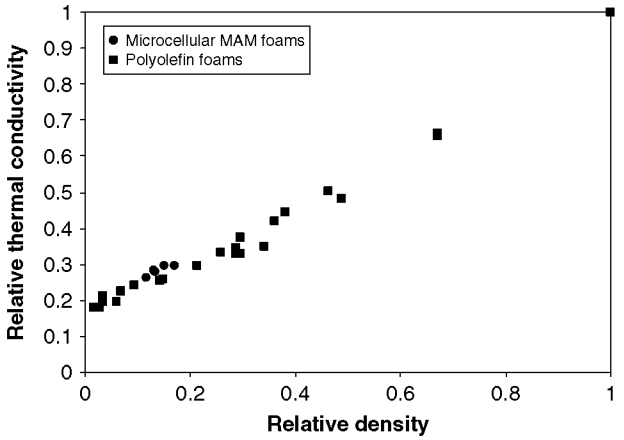

Figure 6. Experimental results for the MAM microcellular foams compared with those for polyolefin-based foams.

If the results for these materials are compared with those previously published for polyolefin-based foams,[32] it can be observed that they follow a very similar trend in terms of relative thermal conductivity (thermal conductivity of the foam divided by the conductivity of the solid) *versus* relative density (Fig. 6). The polyolefin-based foams of the cited paper were not microcellular; therefore these results suggest that the microcellular structure does not play a significant role in the thermal conductivity for MAM foams.

Theoretical modelling of thermal conductivity

The effective thermal conductivity of two-phase materials has been explored using many different approaches.[33] Heat transfer in cellular materials is mainly due to four mechanisms: conduction through the gas phase, conduction through the solid phase, gas convection and radiation. In the absence of heat convection, which is only important for pore sizes greater than 3 mm,[34] the heat transport across a foam having either open or closed cells is dominated by conduction along the polymer matrix, conduction across the gas phase and thermal radiation.

In order to properly understand the measured values for the MAM foams, several theoretical models were used to estimate the thermal conductivity due to conduction mechanisms.

First of all, it is necessary to consider the simplest models: the series–parallel and the parallel–series models which both assume a cubic geometry. In the first, vertical cell walls and gas phase are combined in series to give a two-phase system. To obtain an expression for the whole material, horizontal cells walls are combined in parallel with this two-phase system.[35] In the case of the parallel–series model, the horizontal cell walls are first combined. The final expressions for thermal conduction are the following.

$$\text{Series–parallel model}: \lambda_{gs} = \lambda_s(1 - V_g^{2/3}) + \frac{\lambda_s V_g^{2/3}}{\lambda_g + (\lambda_s - \lambda_g)V_g^{1/3}} \quad (5)$$

$$\text{Parallel–series model}: \lambda_{gs} = \lambda_s \frac{\lambda_s - (\lambda_s - \lambda_g)V_g^{2/3}}{\lambda_s - (\lambda_s - \lambda_g)(V_g^{2/3} - V_g)} \quad (6)$$

where λ_{gs} is the overall conductivity of the foam based on conduction through the combined gas and solid phase, λ_s and λ_g are the conductivities of the solid (aluminium) and gas phase (air), respectively, and V_g is the volume fraction of gas in the cellular material, also called the porosity. It is important to consider that these two models are a combination of the more basic parallel and series models which are not themselves realistic but predict maximum and minimum possible values for thermal conductivity in two-phase systems.

Doherty *et al.*[36] modelled conduction through two-dimensional squared bubbles which represents an advance in comparison with the two models mentioned above.

$$\text{Doherty model}: \lambda_{gs} = \frac{\lambda_s\lambda_g(2V_g + 1) + 2\lambda_s^2(1 - V_g)}{\lambda_g(1 - V_g) + \lambda_s(2 + V_g)} \quad (7)$$

Russell[37] analysed conduction through a solid matrix with cubic cells arranged in line. The cubic pores were assumed to have a uniform cell wall thickness and struts were ignored. The following equation represents an upper limit result for an in-line cubic array of cells.

$$\text{Russell model}: \lambda_{gs} = \lambda_g \left(\frac{V_g^{2/3} + (\lambda_s/\lambda_g)(1 - V_g^{2/3})}{(1 - V_g^{2/3} + V_g) + (\lambda_g/\lambda_s)(V_g^{2/3} - V_g)} \right) \quad (8)$$

Another expression was suggested by Maxwell.[33] He assumed a polyphase composite in which spheres of one phase are randomly dispersed in a second phase (not in line as in the Russell model). The final result of this model is the following.

$$\text{Maxwell model}: \lambda_{gs} = \lambda_g \left(\frac{2V_g + 1 + (\lambda_s/\lambda_g)[2(1 - V_g)]}{(\lambda_s/\lambda_g)(1 - V_g) + (2 + V_g)} \right) \quad (9)$$

A classical model was stated by Lees.[38] The equation that defines the effective thermal conductivity is as follows:

$$\lambda_{gs} = \lambda_g^{V_g} \lambda_s^{(1-V_g)} \quad (10)$$

Gibson and Ashby, based on Glicksman's theoretical assumptions, proposed a theoretical model for closed-cell cellular materials.[39] The final expression obtained by Glicksman is the *lower limit*, i.e. valid for very high porosities. It is important to consider it because nowadays it is one of the most accepted models for the conduction mechanism in thermal conductivity. The expression proposed is the following.

$$\text{Ashby model}: \lambda_{gs} = g\lambda_s(1 - V_g) + \lambda_g V_g \quad (11)$$

where g is an efficiency factor which allows for the tortuous shape of the cell walls and which ranges between 1/3 and 1.

One more empirical model was taken into account.

$$\text{Scaling relation with gas contribution}: \lambda_{gs} = \lambda_s(1 - V_g)^n + \lambda_g V_g \quad (12)$$

where n is usually between 1 and 2.[39]

Figure 7 shows the results of relative thermal conductivity *versus* relative density for all the models considered and for the MAM

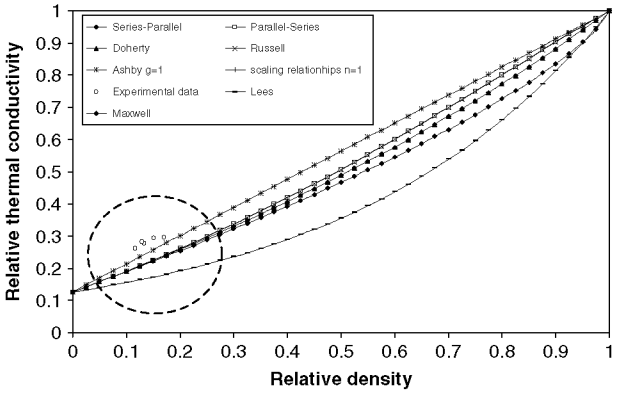

Figure 7. Comparison between experimental results and theoretical models for conduction.

Table 3. Contribution of the radiation term to the thermal conductivity

Relative density	Weighting of radiation term (%)
0.170	6.6
0.152	11.9
0.134	11.9
0.130	14.7
0.117	12.3

microcellular foams. It is important to remark that the theoretical comparison between several models and experimental data is done in a restricted density range. However, from our point of view this theoretical approach has a great utility because most of the models are greatly dependant of relative density that even in such a low range many discrepancies can be presented.

As can be observed, the experimental results are greater than the predictions of any of the equations considered. The values that are closer are those of the Ashby model and the scaling relationships using as fitting factors $g = 1$ (Ashby model) or $n = 1$ (scaling relationships), i.e. the maximum values that these models can predict. This result suggests that there is a contribution from the radiation term for the foams analysed. This contribution has been estimated by subtracting from the experimental results the values given by the Ashby or scaling relationships models.[40] The results are collected in Table 3, where a relative contribution of between 6 and 14% is obtained, which is a typical result for foams with relative densities in the range 0.11–0.17.[32] Therefore, the same conclusion reached when the results were compared with polyolefin foams is found here; the microcellular structure does not improve the thermal insulation capability of the foams under study in comparison to foams with conventional cell sizes. This result can be understood taking into account that the relative densities of the foams are above 0.1, and in this density range the radiation contribution still plays a minor role in the final conductivity. The weight of this contribution could be as high as 25% for foams with relative densities of 0.03.[41] As this heat conduction mechanism is responsible for a reduction of the conductivity when the cell size is reduced, it is credible that no improvements are detected for the materials under study in comparison with conventional foams.

CONCLUSIONS

A collection of microcellular foams, based on a MAM triblock copolymer, were fabricated using supercritical carbon dioxide with a batch process. Controlled cell size and density was achieved by varying the depressurization time, from 60 s to 30 min, leading to cell sizes from 4 to 100 μm and relative densities between 0.11 and 0.17. This result shows the possibility of producing very-low-density microcellular foams maintaining at the same time a very low average cell size. In the case of microcellular foams based on amorphous PMMA, it is shown that although cell size is similar, as presented in the work of Reglero *et al.*,[42] foams based on PMMA present a much higher density that MAM foams (0.8 g cm^{-3} for the PMMA foams and 0.15 g cm^{-3} for the MAM foams). These results show that the nanostructured MAM triblock copolymer allows the combination of low-density foams and very small cell sizes. This can be due to the combination, in a nanostructured assembly, of methacrylate groups with high CO_2 affinity, which ensures a high cell density, with elastic butyl acrylate groups which permits the reaching of low densities during the expansion process.

In addition, a TPS technique was employed to measure the thermal properties of the samples. A decrease of the thermal conductivity was observed in comparison with the solid material, and the influence of the density was also analysed. In addition, several theoretical approaches, based on classical models to predict thermal conductivity in cellular materials, were employed to validate the experimental data. Calculations showed that all the models underestimated the experimental results, which was attributed to the contribution (between 7 and 14%) of the radiation term to the thermal conductivity for these materials. The results demonstrate the possibility of fabricating homogeneous, low-density microcellular MAM foams with well-controlled cell size, and of adjusting the thermal properties to desired values by controlling the foam density.

ACKNOWLEDGEMENTS

Financial assistance from the Local Government Junta of Castile and Leon (Project VA047A07 and Excellence Group GR39), the Spanish Ministry of Science and Education and the FEDER programme (project MAT2006 1614-C03-01) is gratefully acknowledged.

REFERENCES

1 Martini JE, Waldman FA and Suh NP, US Patent 4473665 (1984).
2 Martini JE, Waldman FA and Suh NP, *SPE Tech Pap* **28**:674 (1982).
3 Reverchon E and Cardea S, *J Supercrit Fluids* **40**:144 (2007).
4 Yoon JD and Cha SW, *Polym Test* **20**:287 (2001).
5 Sumarno AR, Bernardus GS, Ismail AS and Putu Teta PA, in *Proceedings of the 8th Meeting on Supercritical Fluids: Chemical Reactivity and Material Processing In Supercritical Fluids*, pp. 467–475 (2002).
6 Arora KA, Lesser AJ and McCarthy TJ, *Macromolecules* **31**:4614 (1998).
7 Jacobs LJM, Danen KCH, Kemmere MF and Keurentjes JTF, *Polymer* **48**:3771 (2007).
8 Uosaki Y, Morokami T and Moriyoshi T, *High Pressure Res* **20**:467 (2001).
9 He Y, Xin C, Li Q and Wang S, *J Beijing Univ Chem Technol (Natural Sci Ed)* **36**:34 (2009).
10 Krause B, Sijbesma HJP, Munuklu P, Van der Vegt FA and Wessling M, *Macromolecules* **34**:8792 (2001).
11 Nayak NC and Tripathy DK, *Cellular Polym* **19**:271 (2000).
12 Murray RE, Weller JE and Kumar V, *Cellular Polym* **19**:413 (2000).
13 Arora KA, Lesser AJ and McCarthy TJ, *Polym Eng Sci* **38**:2050 (1998).
14 Sun H, Sur GS and Mark JE, *Eur Polym J* **38**:823 (2002).
15 Fu J, Choonghee J and Naguib HE, *Cellular Polym* **24**:436 (2005).
16 Gibson LJ and Ashby MF, *Cellular Solids: Structure and Properties*. Cambridge University Press, Cambridge (1997).

17 Rodríguez-Pérez MA, Alonso O, Souto J and de Saja JA, *Polym Test* **16**:4474 (1997).
18 Rindfleisch F, DiNoia TP and McHugh MA, *J Phys Chem* **100**:15581 (1996).
19 Leibler L, *Prog Polym Sci* **30**:898 (2005).
20 Ruzette A-V and Leibler L, *Nature Mater* **4**:19 (2005).
21 Bougerra A, Aït-Mokhtar A, Amiri O and Diop MB, *IntCommun Heat Mass Transfer* **28**:1143 (2001).
22 Saxena NS, Pradeep P, Mathew G, Thomas S, Gustafsson M and Gustafsson SE, *Eur Polym J* **35**:1687 (1999).
23 Almanza O, Rodríguez-Perez MA and de Saja JA, *J Polym Sci B: Polym Phys* **42**:1226 (2004).
24 Solorzano E, Rodríguez-Pérez MA, Reglero JA and de Saja JA, *J Mater Sci* **42**:2557 (2007).
25 Solórzano E, Rodriguez-Perez MA and de Saja JA, *Adv Eng Mater* **10**:596 (2008).
26 Condo PD, Sanchez IC, Panayiotou CG and Johnston KP, *Macromolecules* **25**:6119 (1992).
27 Ito Y, Yamashita M and Okamoto M, *Macromol Mater Eng* **291**:773 (2006).
28 Wong B, Zhang Z and Handa YP, *J Polym Sci B: Polym Phys* **36**:2025 (1998).
29 He Y, Xin C, Li Q and Wang S, *J Beijing Univ Chem Technol (Natural Sci Ed)* **36**:38 (2009).
30 Log T and Gustafsson E, *Fire Mater* **19**:43 (1995).
31 Gustavsson M, Karawacki E and Gustafsson SE, *Rev Sci Instrum* **65**:465 (1994).
32 Solórzano E, Rodriguez-Perez MA, Lázaro J and de Saja JA, *Adv Eng Mater* **11**:818 (2009).
33 Collishaw PG and Evans JRG, *J Mater Sci* **29**:486 (1994).
34 Abramenko AN, Kalinichenko AS, Burster Y, Kalinichenko VA, Tanaeva SA and Vasilenko IP, *J Eng Phys Thermophys* **72**:369 (1999).
35 Leach AG, *J Phys D: Appl Phys* **26**:733 (1993).
36 Doherty JA, Verma RS, Shrivastava S and Saxena SC, *Energy* **11**:773 (1986).
37 Russell RH, *J Am Ceram Soc* **18**:1 (1935).
38 Lees CH, *Philos Mag* **49**:221 (1900).
39 Gibson LJ and Ashby MF, *Cellular Solids*, 2nd edition. Cambridge University Press, Cambridge, pp. 285 – 287 (1997).
40 Rodríguez-Pérez MA, Alonso O, Souto J and de Saja JA, *Polym Test* **16**:287 (1997).
41 Almanza OA, Rodríguez-Pérez MA and de Saja JA, *J Polym Sci B: Polym Phys* **38**:993 (2000).
42 Reglero Ruiz JA, Viot P and Dumon M, *J Appl Polym Sci* **118**:320 (2010).